ISSN 1054-660X, Laser Physics, 2009, Vol. 19, No. 4, pp. 745–751.
© Pleiades Publishing, Ltd., 2009.
Original Text © Astro, Ltd., 2009.

Investigation of Hot Electrons and Hot Phonons Generated within an AlN/GaN High Electron Mobility Transistor

G. Xu[a], S. K. Tripathy[a], X. Mu[a], Y. J. Ding[a], K. Wang[b], Yu. Cao[b], D. Jena[b], and J. B. Khurgin[c]

[a] *Department of Electrical and Computer Engineering, Lehigh University, Bethlehem, PA 18015, USA*
[b] *Department of Electrical Engineering, University of Notre Dame, Notre Dame, IN 46556, USA*
[c] *Department of Electrical and Computer Engineering Johns Hopkins University, Baltimore, MD 21218, USA*
e-mail:yud2@lehigh.edu
Received November 20, 2008

Abstract—We review our recent results obtained on an AlN/GaN-based high-electron-mobility transistor. The temperature of the electrons drifting under a relatively-high electric field is significantly higher than the lattice temperature (i.e., the hot electrons are generated). These hot electrons are produced through the Fröhlich interaction between the drifting electrons and long-lived longitudinal-optical phonons. By fitting electric field vs. electron temperature deduced from the measurements of photoluminescence spectra to a theoretical model, we have deduced the longitudinal-optical-phonon emission time for each electron is to be on the order of 100 fs. We have also measured the decay time constant for LO phonons to be about 4.2 ps. An electric field present in a GaN/AlN heterostructure can bring both the first-order and second-order Raman scattering processes into strong resonances. The resonant Stokes and anti-Stokes Raman scattering results in the increase and decrease of non-equilibrium longitudinal-optical phonon temperatures, respectively. Moreover, the phonon temperature measured from the Raman scattering is increased with an applied electric field at a much higher rate than the lattice temperature due to the presence of field-induced non-equilibrium longitudinal-optical phonons.

PACS numbers: 78.30.-j; 72.10.Di

DOI: 10.1134/S1054660X09040306

1. INTRODUCTION

High-electron-mobility transistors (HEMT's) based on AlGaN/GaN heterostructures have potentials of handling high microwave powers and operating within wide bandwidths [1, 2]. However, the accumulation of the longitudinal-optical (LO) phonons emitted by the electrons drifting in a HEMT may cause the device characteristics to deteriorate. Such an accumulation is due to the fact that LO-phonon emission time for an electron is an order of magnitude shorter than the decay time for the LO phonons. Indeed, using time-resolved backward Raman scattering spectroscopy, the electron-LO-phonon emission time was previously determined to be 50 ± 10 fs [3], which is close to the theoretical estimate of 10 fs [4]. Another approach to deduce the LO-phonon emission time for an electron is to balance the LO-phonon scattering loss per electron [5, 6] and the relaxation rate of the excess energy of the electron system in time domain. Using such a method the LO-phonon emission time was determined to be 0.2 ps [4]. Under a dc electric field, the power loss per electron through its collision with the LO phonon is approximately equal to the power gain per electron drifting under a dc electric field. Therefore, the LO-phonon emission time was also deduced for an *n*-GaN metal-semiconductor field effect transistor [7]. It is worth noting that most of the previous investigations [3, 4, 7] were focused on the bulk-GaN structures. On the other hand, the decay time for the LO phonons into transverse-optical (TO) and acoustic phonons [8] in bulk GaN was measured to be 2.8 ps at room temperature [9]. Therefore, due to the Fröhlich interaction between the long-lived LO phonons and the electrons, the electron temperature is expected to be higher than the lattice temperature, i.e., the generation of hot electrons. These hot electrons and phonons in an AlGaN/GaN channel were investigated using microwave noise technique [10]. Since the LO phonons generated by electrons are accumulated, phonon occupancies are elevated [10–12], i.e., the non-equilibrium or hot phonons are induced. Previously, the hot-phonon temperature and lifetime were estimated from a biased AlGaN/AlN channel based on microwave noise technique [10]. Among different techniques, Raman scattering may be one of the most direct techniques for investigating hot phonons based on the previous result [11].

The accumulation of the hot phonons not only cause electron velocities to saturate but also lead to additional power dissipation [12–15], and therefore, the corresponding electronic devices will deteriorate in time. Even though the GaN-based high-electron-mobility transistor (HEMT) may be the next-generation microwave power amplifiers with the possibilities of handling high powers as well as operating within a wide

[1] The article is published in the original.

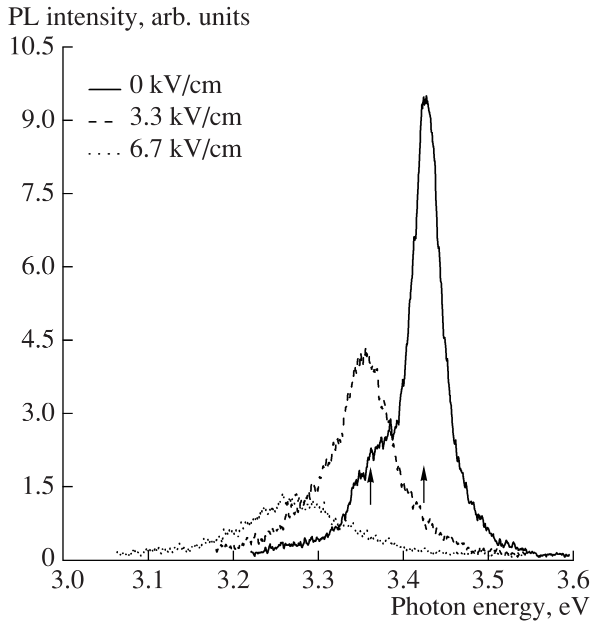

Fig. 1. Photoluminescence spectra measured on an AlN/GaN-based HEMT structure at an excitation wavelength of 208 nm for three different dc electric fields. Arrows mark two transition peaks under the zero electric field.

bandwidth [16], hot phonons could impose a fundamental limit to the performance of a GaN-based HEMT.

In this proceedings article, we review our results published recently [17] based on our investigation of the hot electrons generated in a biased AlN/GaN HEMT in a photoluminescence experiment. We show that the hot electrons are produced as a result of the Fröhlich interaction between the long-lived LO phonons and the electrons drifting in the HEMT and also determine the LO phonon emission time. We will also review our results published in [18] following the investigation of the non-equilibrium LO phonons in a biased GaN/AlN heterostructure based on first-order and second-order resonant Raman scattering.

2. AlN/GaN HIGH ELECTRON MOBILITY TRANSISTOR

An AlN/GaN-based HEMT, grown by molecular beam epitaxy, consists of a 4-nm AlN, a 200-nm unintentionally-doped GaN layer, a semi-insulating GaN layer, and a GaN-on-sapphire template layer (from top to bottom). A patterned metallic film was evaporated onto the A1N layer. Source and drain ohmic contacts were formed by the evaporation of the gold film followed by annealing. For this work, the distance between the source and drain was 30 ∝m and there is no gate present. Due to the spontaneous and strain-induced piezoelectric polarizations [2], a two-dimensional electron gas with a high electron density was confined within the GaN layer in the proximity of the GaN/AlN interface. At room temperature, the sheet electron concentration and the electron mobility were measured to be 2.5×10^{13} cm^{-2} and 1200 cm^2/V s, respectively.

3. INVESTIGATION OF HOT ELECTRONS

Photoluminescence (PL) spectra emitted by the HEMT were measured when the device was pumped by a 3-ps pulsed coherent radiation at the wavelength of 208 nm. Such a pump beam was the output of quadrupling the frequency of the laser pulses at a central wavelength of 832 nm using two β-BaB_2O_4 crystals. The maximum output power of the pump beam was measured to be 3 mW. During our experiment, however, the average power of the pump beam focused on the samples surface was fixed to 1 mW. At such a pump power, the effect of the pump-induced HEMT heating was negligible. The PL intensity was collected at room temperature for different voltages between the source and drain in the range of 0–30 V. The collected PL signal was sent through a double monochromator and then detected by a photomultiplier tube. A lock-in amplifier was used to reduce the noise of our measurements.

Figure 1 shows the typical PL spectra taken at room temperature. At the zero bias between the source and drain of the HEMT, the PL spectrum is primarily dominated by recombination between electrons and holes in the GaN/AlN channel at 3.425 eV (362 nm) [19]. A shoulder at 3.362 eV can be attributed to recombination of excitons in the GaN/AlN channel. With increasing the bias (the corresponding electric field given by the ratio of the bias and the distance between the source and drain), the PL spectrum became more and more broadened while the emission peak was significantly red-shifted. The red-shift of the dominant PL emission peak was caused by joule heating of the device due to the applied bias voltage through the HEMT (the current can be as high as 85 mA at 30 V). When the electric field was increased, the photogenerated electrons and heavy holes drifted towards the opposite directions. Consequently, the recombination rate between these electrons and heavy holes was subsequently reduced. According to [20], the transition energy of excitons in bulk GaN is given by:

$$E_g(T_l) = E_g(0) - 9.09 \times 10^{-4} T_l^2/(830 + T_l), \quad (1)$$

where $E_g(0)$ is the bandgap of GaN at 0 K and T_l is the lattice temperature. According to [21], we fitted the low-energy side of each PL spectrum by using $I_{PL} \propto \sqrt{E - E_g}$, and therefore, obtained the bandgap (E_g) at each bias. Substituting the resulting bandgap at the zero bias into Eq. (1), we obtained $E_g(0) \approx 3.468$ eV. This value is 42 meV lower than the accepted value of 3.510 eV [20]. Such a difference may be caused by bandgap renormalization due to the high-density electrons present in the AlN/GaN channel. Indeed, in our

sample the sheet density of electrons was measured to be 2.5×10^{13} cm^{-2}, which is sufficiently high for causing the effective bandgap to shrink by 42 meV [22]. For the rest of the biases applied to the HEMT, we then used Eq. (1) to determine the corresponding lattice temperatures, see Fig. 2. The obtained lattice temperatures are in a good agreement with the photoluminescence measurements at high temperatures [23].

Since the effective mass for electrons is much smaller than that for the heavy holes, photogenerated electrons gain much higher kinetic energies than the heavy holes. Consequently, these electrons not only drift under the dc electric field but also emit and absorb LO phonons through the Fröhlich interaction. Besides the interaction between electrons and LO phonons, the collision between electrons brings the electrons to an equilibrium at the electron temperature (T_e). The electron temperature for the nondegenerate electrons, can be determined by fitting each

PL intensity spectrum on the high-energy side using the following dependence [6, 21]:

$$I_{\mathrm{PL}} \propto e^{-(E-E_g)/kT_e}. \qquad (2)$$

For the PL spectrum measured by us at each bias, we have determined the corresponding value of T_e, see Fig. 2. It is worth noting that the hot-electron temperatures obtained by us are in the same order of magnitude as that determined previously [10]. According to Fig. 2, the electron temperature is quite close to the lattice temperature for the dc electric field less than 5 kV/cm. Above such a value, however, the electron temperature is significantly higher than the lattice temperature, see Fig. 2. This is due to the fact that as the electric field is increased the kinetic energies of the electrons are increased. These more energetic electrons then emit and absorb more LO phonons. Since the LO-phonon emission time for an electron is much shorter than the decay time of the LO phonons, the LO phonons become accumulated in time, which results in the increase of the phonon temperature. Consequently, the electron temperature is also increased.

Under our experimental condition the scattering of the electrons by acoustic phonons is negligible. Therefore, we assume that the dominant mechanism for the energy loss of the electrons at room temperature is the scattering of the electrons by LO phonons. Under such a case, the power-loss per nondegenerate electron is given by [5]

$$P(T_e)_{\mathrm{LO}} = \frac{\hbar\omega_{\mathrm{LO}}}{\tau_{e\text{-ph}}}\left(\frac{e^{(x_0-x_e)}-1}{e^{(x_0)}-1}\right) \times\left[\frac{(x_e/2)^{1/2}e^{x_e/2}K_0(x_e/2)}{\sqrt{\pi/2}}\right], \qquad (3)$$

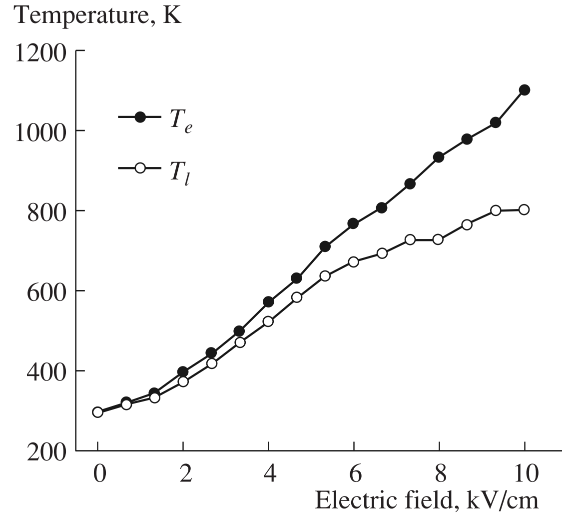

Fig. 2. Electron temperature (filled dots) and lattice temperature (open circles) under different electric fields, deduced from PL spectra, see Fig. 1.

where $\hbar\omega_{\mathrm{LO}}$ = 91.8 meV is the LO phonon energy for GaN, $\tau_{e\text{-ph}}$ is the LO-phonon emission time for an electron, $x_e = \hbar\omega_{\mathrm{LO}}/k_{\mathrm{B}}T_e$, and $x_0 = \hbar\omega_{\mathrm{LO}}/k_{\mathrm{B}}T_l$ with k_{B} the Boltzmann constant and K_0 is the modified Bessel function of zero order. Under the steady state, the power loss given by Eq. (3) should be approximately equal to the power gain for an electron from the dc electric field. As a result, one can obtain an expression for the dc electric field applied to the HEMT:

$$E_{dc} = \sqrt{P(T_e)_{\mathrm{LO}}/(e\propto_e)}, \qquad (4)$$

where e is the charge of an electron and $\propto_e$ is the mobility of the electrons.

According to Eq. (4), the dc electric field is as a function of $\tau_{e\text{-ph}}$ whereby T_e and T_l can be replaced by the values deduced from the PL spectra, see Fig. 2. Such a function was then used by us to achieve a nonlinear-least-square fit to the values of the electric fields calculated by the bias applied to the HEMT divided by 30 ∝m, see Fig. 3. As a result, the LO phonon emission time for an electron was obtained to be on the order of 100 fs. This value lies between those determined based on time-resolved backward Raman scattering spectroscopy (i.e., 50 ± 10 fs) [3] and using a similar approach under the zero electric field (0.2 ps) [4] for the bulk GaN. Our value of the LO phonon emission time is much higher than the theoretical value of 10 fs. Such a disprepancy may be caused by the screening of electron-phonon interaction due to the presence of the high-density electrons in a two-dimensional HEMT [24]. The rate of the energy dissipation for the hot electrons is reduced by the re-absorption of the hot phonons [14], which may increase the emission time of the LO phonons.

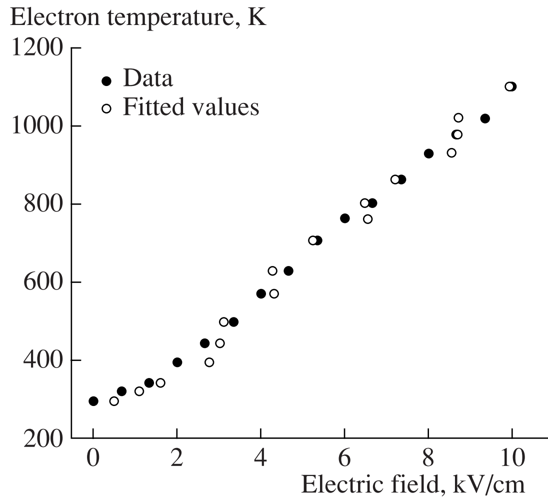

Fig. 3. Electron temperature vs. electric field: data (filled dots)—deduced from the PL spectra, see Fig. 1; fitted values (open circles)—after fitting data using Eq. (4).

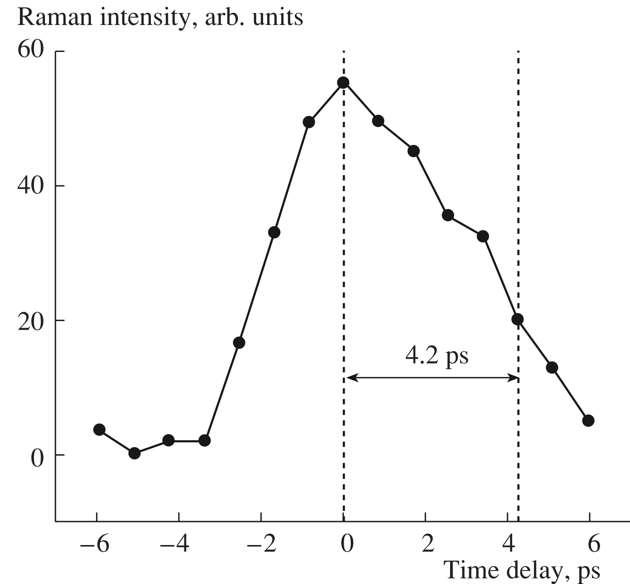

Fig. 4. Raman intensity is measured vs. time delay for pump pulses relative to probe pulses.

4. EVIDENCE OF HOT PHONONS

A Raman signal scattered by the A1N side of the HEMT backward was collected by a two-stage cascaded monochromator at room temperature (295 K) at different biases applied between the source and drain in the range of 0–36 V. The outgoing Raman signal was then measured using a photomultiplier tube after going through the monochromator. A coherent picosecond radiation with the output wavelength in the range of 369–385 nm, produced by frequency-doubling a mode-locked picosecond Ti:sapphire laser output in a 10-mm-thick BBO crystal, was used as an incident beam. The width of each incident pulse was measured to be 3 ps. During each measurement, a typical average incident power of 30 mW was used. The incident beam was focused down to the HEMT with a beam radius of ~150 ∝m. The lattice temperature of the HEMT under a fixed bias was deduced by fitting the photoluminescence (PL) spectral profiles on the low-energy side, generated by a picosecond coherent UV radiation, by using Boltzmann distribution [21]. As a result, we obtained the bandgap, $E_g(T)$, for the GaN channel at each fixed DC electric field. Using [20], we deduced the corresponding DC lattice temperature. We also measured the decay time of the LO phonons [8] to be about 4.2 ps using pump-probe technique at the incident wavelength of 380 nm, see Fig. 4. This value is consistent with 2.8 ps measured previously [9].

The temperatures of the LO phonons are determined to be:

$$T_{1\mathrm{LO}} = \frac{\hbar\omega_{\mathrm{LO}}}{k_{\mathrm{B}}\ln[(n^{(1)}+1)/n^{(1)}]}, \quad (5)$$

where $n^{(1)}$ is the phonon occupation number determined from the first-order Raman scattering [11]. The two peaks resolved in Fig. 5 correspond to the first-order and second-order Raman scattering of the picosecond incident pulses by the LO phonons with their energies being $\hbar\omega_{\mathrm{LO}} \approx 91.8$ meV in the GaN channel layer. At different electric fields or incident photon energies the intensities for the first-order and second-order Stokes and anti-Stokes Raman scattering are different, see Fig. 6. Each of the four Raman scattering processes is going through its own resonance at a specific electric field.

One can see from Fig. 6 that for the first-order Raman scattering there are two dominant peaks labeled by $P_{AS}^{(1)}(0)$ and $P_S^{(1)}(1)$ corresponding to the anti-Stokes and Stokes Raman scattering at $E_i - E_g \approx 3$ meV and $E_i - E_g \approx 80$ meV, respectively. According to [20], these two peaks correspond to the resonances for the incoming and outgoing photons to the bandgap of the GaN channel, respectively. A tail $P_{AS}^{(1)}(-1)$ and a shoulder $P_S^{(1)}(0)$ can be attributed to the anti-Stokes and Stokes Raman scattering at $E_i - E_g \approx -96$ meV and $E_i - E_g \approx 0$ meV, respectively. They correspond to the resonances of the outgoing and incoming photon energies to the bandgap, respectively. The resonance for the incoming photons $P_S^{(1)}(0)$ is much weaker than that for the outgoing photons $P_S^{(1)}(1)$. For the resonance of the outgoing photons, free excitons are generated by the incoming photons, which further enhance the Raman signal intensities (i.e., a double resonance). For the first-order anti-Stokes Raman scattering, however, the

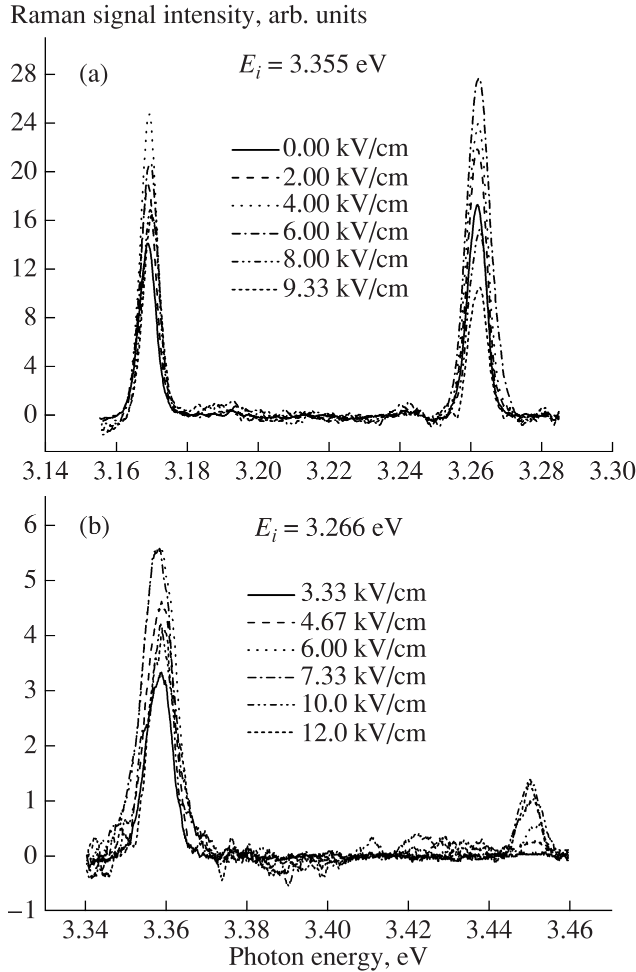

Fig. 5. Spectra of first-order and second-order (a) Stokes and (b) anti-Stokes Raman scattering at different electric fields indicated. E_i is used to designate the photon energy of the incident beam.

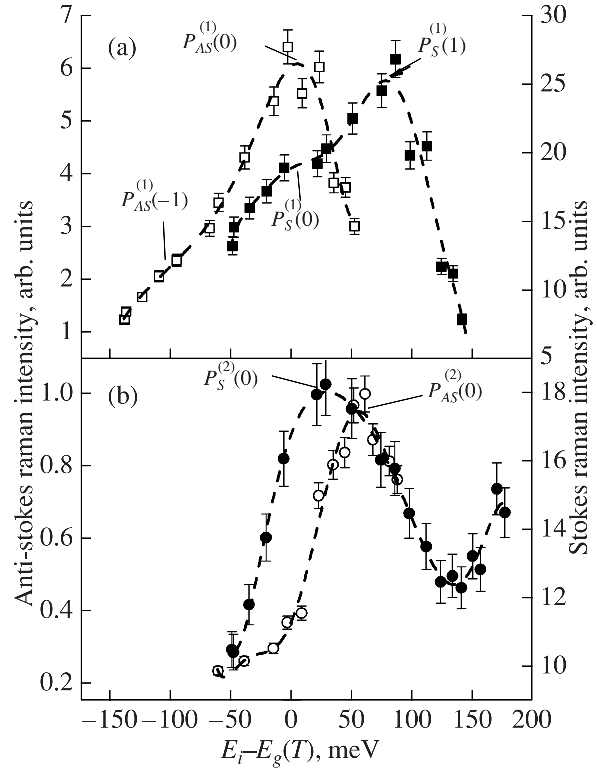

Fig. 6. Dependences of (a) first-order and (b) second-order Raman-scattering signal intensities deduced from Fig. 5, on the photon energy of the incident beam measured relative to the bandgap of GaN. Filled squares and filled circles—Stokes; open squares and open circles—anti-Stokes. All dashed curves correspond to fitting to data. Errors are indicated in the figures.

resonance for the incoming photons $P_{AS}^{(1)}(0)$ is much stronger than that for the outgoing photons $P_{AS}^{(1)}(-1)$. Such behaviors are quite different from [25]. In our heterostructure the generation of the electrons and their subsequent drift in a dc electric field have further enhanced $P_{AS}^{(1)}(0)$ and $P_{AS}^{(1)}(1)$.

One can see from Fig. 6b that for the second-order Raman scattering two resonant peaks, labeled as $P_S^{(2)}(0)$ and $P_{AS}^{(2)}(0)$, are located at $E_i - E_g(T) \approx 27$ and ≈ 56 meV, respectively. In our experiment, without applying a bias to the GaN/AlN heterostructure, we could not observe any second-order anti-Stokes Raman signal regardless of the detuning. After applying a relatively high electric field, the second-order anti-Stokes Raman peak becomes obvious. Moreover, the Raman signal can be significantly enhanced as the electric field is further increased, see Fig. 5. Such an enhancement caused by the increase of the electric field is an evidence for the presence of the hot phonons. For the second-order Raman scattering, two LO phonons must be absorbed or emitted simultaneously. The increase in the Raman signal intensity starting at $E_i - E_g(T) \approx 150$ meV in Fig. 6 could be caused by a resonant peak for the Stokes Raman scattering at $E_i - E_g(T) \approx 184$ meV (i.e., twice the LO phonon energy).

Using Eq. (5), we have determined the phonon temperatures from the first-order Raman scattering. For the incident photon energies of 3.355 eV and 3.266 eV, the phonon temperature increases at almost the same rate as the lattice temperature for the electric fields in the range of 0–5.33 kV/cm, see Fig. 7. Within such a range the increase of the electric field results in the increase of the lattice temperature, and therefore, the increase the phonon temperature. Above 5.33 kV/cm, however, the increase in the phonon temperature is much steeper than that in the lattice temperature, see Fig. 7. This implies that in such a range the increase in the electric field leads to the generation of additional LO phonons within 3 ps above those determined from the thermal equilibrium at the lattice temperature. Assuming that an electron is accelerated from zero kinetic energy to $\hbar\omega_{LO}$

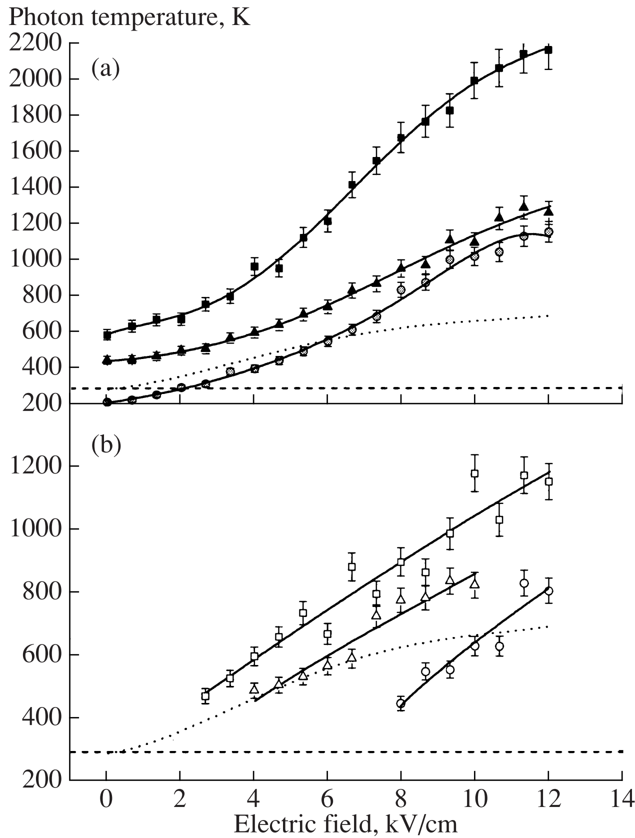

Fig. 7. LO photon temperatures vs. electric field, deduced from (a) first-order (filled symbols) and (b) second-order (open symbols) Raman scattering, as a function of the electric field at three different sets of photon energies for the incident beam: 3.361 and 3.270 eV (filled and open squares); 3.355 and 3.266 eV (filled and open triangles); 3.316 and 3.225 eV (filled and open circles). Solid curves, dotted curves, and horizontal dashed lines correspond to fitting to data, lattice temperatures, and room temperature (i.e., 295 K), respectively. Errors are indicated in the figures.

under an electric field of E_{dc}, one can then estimate the duration of the acceleration to be 0.86 ps. This value is in the same order of magnitude as the decay time constant for the LO phonons [9]. Therefore, the LO phonons generated by the drifting electrons are excessively accumulated. Based on our experimental result (Fig. 7), the highest phonon temperature is determined to be 1290 K at the electric field of 11.3 kV/cm, which is higher than the lattice temperature by 583 K.

On the other hand, the phonon temperatures determined from the second-order Raman scattering are considerably lower, see Fig. 7b. According to [26], the wave-vectors of the two LO phonons participating in the second-order Raman scattering must obey a simple selection rule of $\mathbf{q}_1 + \mathbf{q}_2 = \mathbf{k}_L - \mathbf{k}_S$ due to conservation of momentum. Therefore, the LO phonons within the entire Brillouin zone participate in such a process. In such a case, the phonon temperature deduced from the second-order Raman scattering represents an average temperature for the LO phonons within the entire Brillouin zone. In contrast, for the first-order Raman scattering only the LO phonons with the proper values of the wave vectors participate in the process since $\mathbf{q} = \mathbf{k}_L - \mathbf{k}_S$. At a relatively low electric field, the phonon temperature, T_{2LO}, is about the same as the corresponding lattice temperature, see Fig. 7b. As the electric field is increased, however, the phonon temperature becomes higher than the lattice temperature. However, it is increased at a rate much lower than that for the first-order Raman scattering, see Fig. 7. The highest phonon temperature is 839 K at the electric field of 9.33 kV/cm. In comparison, the phonon temperature determined from the first-order Raman scattering at the same electric field is 1110 K.

According to Fig. 7b, it appears to us that the rates of the increases in the phonon temperatures are significantly less than those determined from the first-order Raman scattering. Since two LO phonons are simultaneously absorbed or emitted for the second-order Raman scattering, the temperature determined from the second-order Raman scattering represents an average value over the LO phonons within the entire Brillouin Zone. This is the reason why the increases in the phonon temperatures as the incident photon energies are increased, determined from the second-order Raman scattering, should be much less. According to Fig. 7b, the lowest electric field measured at which the second-order anti-Stokes Raman peak is observable is decreased as the photon energy is increased, which can be viewed as an evidence on the generation of the hot LO phonons by the picosecond incident pulses.

5. CONCLUSIONS

In conclusion, we have investigated hot-electron effects in an AlN/GaN-based HEMT structure. Through the measurements of PL spectra at different dc electric fields, we have observed that the electron temperature can be significantly above the lattice temperature. Such hot electrons are generated as a result of the Frohlich interaction between the electrons drifting under a dc electric field and long-lived longitudinal-optical phonons. By assuming that the power loss and gain balance out, we have deduced the LO-phonon emission time for each electron to be on the order of 100 fs. We have also measured the decay time for the LO phonons to be about 4.2 ps. These values are within the same order of magnitude as those determined previously for the bulk GaN.

We have also investigated the non-equilibrium LO phonons caused by the first-order Stokes and anti-Stokes resonant Raman scattering in the presence of an electric field in a GaN/AIN heterostructure. By increasing the electric field to a relatively high value, the non-equilibrium LO phonons are generated by the electrons drifting in the electric field. The phonon temperatures deduced from the first-order Raman are much higher

than the corresponding lattice temperatures whereas those deduced from the second-order Raman are considerably lower.

ACKNOWLEDGMENTS

We are indebted to Dr. M. J. Rosker for valuable discussions. This work has been supported by DARPA through AFOSR.

REFERENCES

1. H. Xing, S. Keller, Y.-F. Wu, L. McCarthy, I. P. Smorchkova, D. Buttari, R. Coffie, D. S. Green, G. Parish, S. Heikman, L. Shen, N. Zhang, J. J. Xu, B. P. Keller, S. P. DenBaars, and U. K. Mishra, J. Phys.: Cond. Mat. **13**, 7139 (2001).
2. U. K. Mishra, Y.-F. Wu, B. P. Keller, S. Keller, and S. P. DenBaars, IEEE Tran. Micro. Theo. Tech. **46**, 756 (1998).
3. K. T. Tsen, D. K. Ferry, A. Botchkarev, B. Sverdlov, A. Salvador, and H. Morkoc, Appl. Phys. Lett. **71**, 1852 (1997).
4. H. Ye, G. W. Wicks, and P. M. Fauchet, Appl. Phys. Lett. **74**, 711 (1999).
5. E. M. Conwell in *High Field Transport in Semiconductors*, Solid State Physics, Suppl. 9, Ed. by F. Seitz, D. Turnbull, and H. Ehrenreich (Academic, New York, 1967), p. 159.
6. J. Shah, Sol. State Electron. **21**, 43 (1978).
7. K. Wang, J. Simon, N. Goel, and D. Jena, Appl. Phys. Lett. **88**, 022103 (2006).
8. B. K. Ridley, J. Phys.: Condens. Matter **8**, L511 (1996).
9. K. T. Tsen, D. K. Ferry, A. Botchkarev, B. Sverdlov, A. Salvador, and H. Morkoc, Appl. Phys. Lett. **72**, 2132 (1998).
10. A. Matulionis, J. Liberis, I. Matulionienė, M. Ramonas, L. F. Eastman, J. R. Shealy, V. Tilak, A. Vertiatchikh, Phys. Rev B **68**, 035338 (2003).
11. K. T. Tsen, K. R. Wald, T. Ruf, P. Y. Yu, and H. Morkoc, Phys. Rev. Lett. **67**, 2557 (1991).
12. B. K. Ridley, W. J. Schaff, and L. F. Eastman, J. Appl. Phys. **96**, 1499 (2004).
13. C. H. Oxley, M. J. Uren, A. Coates, and D. G. Hayes, IEEE Tran. Electron Dev. **53**, 565 (2006).
14. M. Ramonas, A. Matulionis, J. Liberis, L. Eastman, X. Chen, and Y.-J. Sun, Phys. Rev B **71**, 075324 (2005).
15. J. Khurgin, Y. J. Ding, and D. Jena, Appl. Phys. Lett. **91**, 252104 (2007).
16. T. Palacios, A. Chakraborty, S. Heikman, S. Keller, S. P. DenBaars, and U. K. Mishra, IEEE Electron Dev. Lett. **27**, 13 (2006).
17. S. K. Tripathy, G. Xu, X. Mu, and Y. J. Ding, K. Wang, C. Yu, D. Jena, and J. B. Khurgin, Appl. Phys. Lett. **92**, 013513 (2008).
18. G. Xu, S. K. Tripathy, X. Mu, Y. J. Ding, K. Wang, Y. Cao, D. Jena, and J. B. Khurgin, Appl. Phys. Lett. **93**, 051912 (2008).
19. Z. Wang, K. Reimann, M. Woerner. T. Elsaesser, D. Hofstetter, J. Hwang, W. J. Schaff, and L. F. Eastman, Phys. Rev. Lett. **94**, 037403 (2005).
20. X.-B. Chen, J. Huso, J. L. Morrison, and L. Bergman, J. Appl. Phys. **99**, 046105 (2006).
21. I. Vurgaftman and J. R. Meyer, J. Appl. Phys. **94**, 3675 (2003).
22. D.-S. Kim and P. Y. Yu, Phys. Rev. B **43**, 4158 (1991).
23. T. Nagai, T. J. Inagaki, and Y. Kanemitsu, Appl. Phys. Lett. **84**, 1284 (2003).
24. N. Nepal, K. B. Nam, J. Li, M. L. Nakarmi, J. Y. Lin, and H. X. Jiang, Appl. Phys. Lett. **88**, 261919 (2006).
25. A. Matulionis, J. Liberis, M. Ramonas, I. Matulionienė, L. F. Eastman, A. Vertiatchikh, X. Chen, and Y.-J. Sun, Phys. Status Solidi C **7**, 2585 (2005).
26. J. Reydellet, P. Y. Yu, J. M. Besson, and M. Balkanski, in *Physics of Semiconductors 1978*, Ed. by B. L. H. Wilson (Inst. of Phys., Bristol, UK, 1979), pp. 1271–1274.
27. A. G. Cristóbal, A. Cantarero, C. T. Giner, and M. Cardona, Phys. Rev. B **49**, 13430 (1994).